Optics and Lasers in Engineering 160 (2023) 107284

Contents lists available at ScienceDirect

Optics and Lasers in Engineering

journal homepage: www.elsevier.com/locate/optlaseng

# Robot-assisted laser ablation for 3D surfaces. Application for paint removal with ultrashort pulse laser

Angel Rodríguez, Ana J. López*, Javier Lamas, Alicia Moreno, Alberto Ramil

*Laboratorio de Aplicacións Industriais do Láser (CITENI). Campus Industrial de Ferrol. Universidade da Coruña, 15471 Ferrol Spain*

ARTICLE INFO

*Keywords:*
3D laser processing
Robotic manipulator
Automation
Ultrashort pulse laser
Laser scanning
Paint removal

ABSTRACT

In this work, a robot-assisted laser cleaning system is presented that allows the automatic processing of 3D objects with arbitrary geometry. The system is based on the integration of a femtosecond pulse laser with a 6-degree-of-freedom (6 DOF) robotic arm and a laser profilometer to capture the geometry of the workpiece. An automatic procedure is performed to generate cleaning paths over the geometry, which is finally targeted by a laser source by means of the prescribed robot motion; thus, both the working distance and the normal incidence of the laser beam are kept fixed for each point on the surface. The manipulator allows displacements and changes of orientation of the object to be processed following the programmed paths in a full 3D solution. The system was tested by performing the cleaning over different curved painted metal surfaces. Experimental results show the effectiveness of the proposed method that improves the efficiency of the automatic laser cleaning of 3D objects and further promotes its application to other ablation processes.

## 1. Introduction

Laser cleaning is a well-known method to remove particles or contaminants from a solid surface [1]. This ablative technique has attracted the efforts of multiple researchers and has been applied in different sectors - from heavy industrial environments such as the automotive and aerospace industries, to areas such as medicine or electronics [2–5], the removal of radioactive pollution from nuclear power facilities [6,7], or the conservation of cultural heritage [8–11], among others. Laser cleaning is a versatile technique, which allows greater precision and control than conventional techniques, and replaces conventional chemical and abrasive processes for the removal of coatings, oxides, paints, and, in general, unwanted layers from a solid substrate by favouring compliance with the environmental, efficiency and quality requirements of the process.

Conventional nanosecond-duration laser pulses are widely used for paint cleaning, however femtosecond-duration pulse lasers have the capability to ablate material from the surface without heat propagation into the bulk; thus heat sensitive materials such as glass or polymer composites can be processed by femtosecond lasers with high precision and minimal thermal and thermomechanical damage [12]. Initial research using femtosecond laser pulses to remove biological crusts from ornamental granitic stone demonstrated that femtosecond lasers generated less heat in the stone substrate than longer pulse durations, and showed high cleaning efficiency [13]. In any case, regardless of the type of laser, the successful outcome of the laser cleaning depends on the material properties of the contaminant and the substrate and also of the laser parameters, such as angle of incidence, laser fluence, or the number of pulses used. These parameters have a great impact on the effectiveness of cleaning and the prevention of unwanted damage to the underlying surface.

In this sense, it has been previously reported [14] that for the uniform cleaning of planar surfaces, laser fluence, and scanning speed must remain constant over the whole surface. These requirements are also common in other laser processes in which a great deal of precision is needed, as for example in laser machining, laser texturing, or laser polishing [15–19]. For this, the distance from the focus to the surface have to be kept constant, but also the laser beam must hit perpendicularly the surface. In oblique incidence, the laser spot becomes elliptical and the energy deposited at the surface is different according to the main directions of the ellipse; consequently, the laser processing is not uniform [20]. Lack of control of the laser conditions at the target surface can cause poor removal of the contaminating layer in some areas due to insufficient energy applied and possible substrate damage in other areas due to laser overexposure [17]. In the case of curved surfaces, meeting these conditions is still a challenge.

Recently, various approaches to the laser processing of 3D surfaces have been published; a common strategy is to divide the surface into

* Corresponding author.
*E-mail address:* ana.xesus.lopez@udc.es (A.J. López).

https://doi.org/10.1016/j.optlaseng.2022.107284
Received 10 June 2022; Received in revised form 18 August 2022; Accepted 12 September 2022
Available online 19 September 2022

multiple sub-regions that are processed as flat surfaces. Galvanometer scanner systems are typically used to quickly guide the laser over these areas [21,22]. This method, however, is viable only for surfaces of low curvature, in which the errors caused by the approximation by planes are small. In addition, since the regions are processed individually, the surface finish can present discontinuities in the overlapping areas of the subregions. In most studies, a 2.5D/quasi-3D approach is used and either the object to be processed or the laser source is moved using positioners with less than 6 degrees of freedom to make it possible to maintain the laser focus at a specific distance of the surface but not the angle of incidence [23]. This simplification does not allow surfaces with high curvature to be optimally processed since the laser beam can be greatly distorted [24]. Moreover, most of the studies assume that the geometry of the object to be processed is known a priori. This approach is acceptable when the target workpieces are mass-produced following a standardized process, with minimum changes in geometry involved and digital models of the surface available. However, when dealing with custom objects or when their location in the workspace is unknown, their geometry must be retrieved to generate the correct tool paths.

Multiple techniques exist to obtain the geometry of an object [25]. The use of one or the other depends on multiple factors, such as the size of the object to be measured, the desired spatial resolution, or the characteristics of the analysed material. For the 3D scanning of macroscopic objects, the most popular methods are optical, among which laser triangulation and structured light techniques stand out [26]. With current acquisition technology, usually the digitized models of the objects cannot be used directly due to the presence of scanning artefacts, such as noise, outliers, or holes in the geometry [27]. In most cases it is, therefore, necessary to post-process the geometry, which is usually a semi-manual and laborious process. The development and application of modern techniques for point cloud processing and surface reconstruction is a key point for 3D scanning technologies to become mainstream [28]. The number of studies in which laser cleaning has been applied altogether with digital geometry acquisition is scarce. Our group used a laser triangulation profilometer to scan and subsequently clean uneven stone surfaces [29]. The results showed an improvement in results when using the 3D processing system with respect to 2D trajectories. Studies can also be found in other fields of application of laser technology, such as repair [30,31] and manufacturing [32–34], laser machining and marking [35,36], and laser cutting [37].

On the other hand, industrial robot manipulators are highly versatile compared to traditional CNC machines when it is necessary to work with objects with complex surfaces, since, in general, they have a greater range of movements. In addition, modern controllers allow the user to integrate different sensors and actuators into the movement system according to process requirements. One of the main disadvantages of robot manipulators compared to traditional CNC machines is that its programming is generally more involved. In the vast majority of industrial applications, this drawback is mitigated since the robot on assembly lines typically executes the same repetitive movements over and over. However, to process objects on demand, the user has to calculate the movement of the manipulator for each case or develop a code that does it automatically for each case. This is a great barrier to entry for many potential users and limits the popularization of these types of systems outside of their well-established fields. It is, therefore, important to move towards the development of automatic integrated systems that allow complex processing tasks to be performed as easily as possible.

In this work, a solution for the controlled laser ablation process of arbitrary 3D objects has been developed, which consists of the integration of a 6 DOF robotic arm, an ultrashort pulse laser, and a vision system to obtain a digital model of the object to be processed. Once the model of the surface was retrieved and processed, three-dimensional tool trajectories were calculated over the geometry. The robot manipulator was used to move the object relative to the laser beam along the prescribed trajectories in order to process the surface. The use of a manipulator robot allowed precise control of the position, orientation, and relative speed between the beam and the target surface. This setup was applied to laser paint stripping of samples with different geometries. To evaluate the performance of the system, different cleaning strategies were tested; the results obtained regarding the degree of paint removal confirmed the improvement in the quality of the laser processing that is achieved with the developed system.

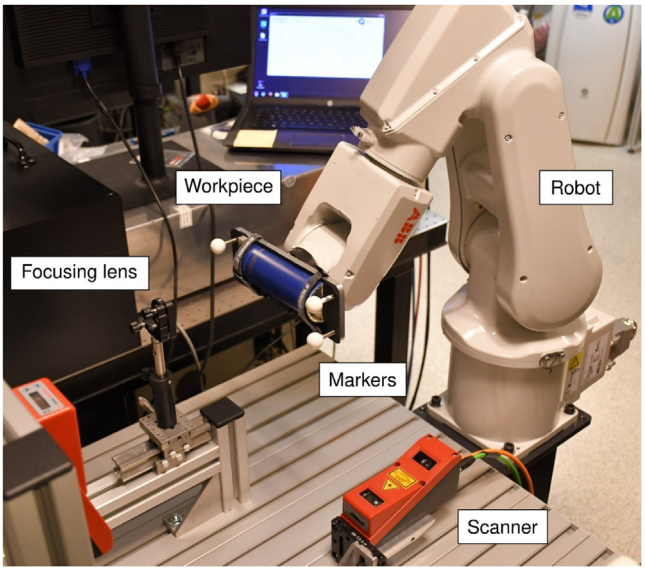


**Fig. 1.** Experimental setup. The main components of the laser cleaning system are shown in the image.

## 2. Materials and methods

### 2.1. Experimental setup

The experimental setup is shown in Fig. 1. A six-axis robot ABB IRB 120 was used as the manipulator. The object to be processed was fixed to a plate attached to the end effector of the robot arm. The robot had a horizontal reach of 0.58 m and its repetition in position is 0.01 mm. A Leuze Electronic LPS 36 laser scanner was used to acquire the geometry of the object. The scanner projects a laser line onto the surface, and a profile with the coordinates of the line can be obtained by triangulation of the reflected light. The resolution of the scanner is between 0.5 mm and 1.5 mm for the X-axis (longitudinal direction of the projected line) and between 0.5 mm and 3 mm for the Z-axis (height value). The profiles were acquired at a frequency of 100 Hz.

The laser cleaning system consists of a femtosecond pulsed near-infrared laser, and specifically the Spirit system by Spectra-Physics, with an emission wavelength of 1040 nm and pulse width of 396 fs. The intensity profile at the laser output was near-Gaussian ($M2 < 1.2$) and the diameter of the beam was 1.5 mm with horizontal polarisation (>100:1). The pulse rate can be set from a single shot to 1 MHz, with a maximum pulse energy of 40 $\mu J$ at 100 kHz. The maximum mean power output is > 4 W. The laser beam is focused on the surface of the workpiece using a lens, 150 mm focal length, to a minimum spot diameter of roughly 40 μm when the focus is located right on the surface.

All devices are interconnected with each other to allow communication during operation. A computer runs a custom-developed application that sends execution orders to the robot controller and to the laser scanner and receives information from them via TCP/IP and UDP protocols. The power regulation and activation of the femtosecond laser is controlled by an analog and a digital input, respectively. These signals are generated from the robot controller and a programmable controller is used to adjust their levels to the values required by the laser system.

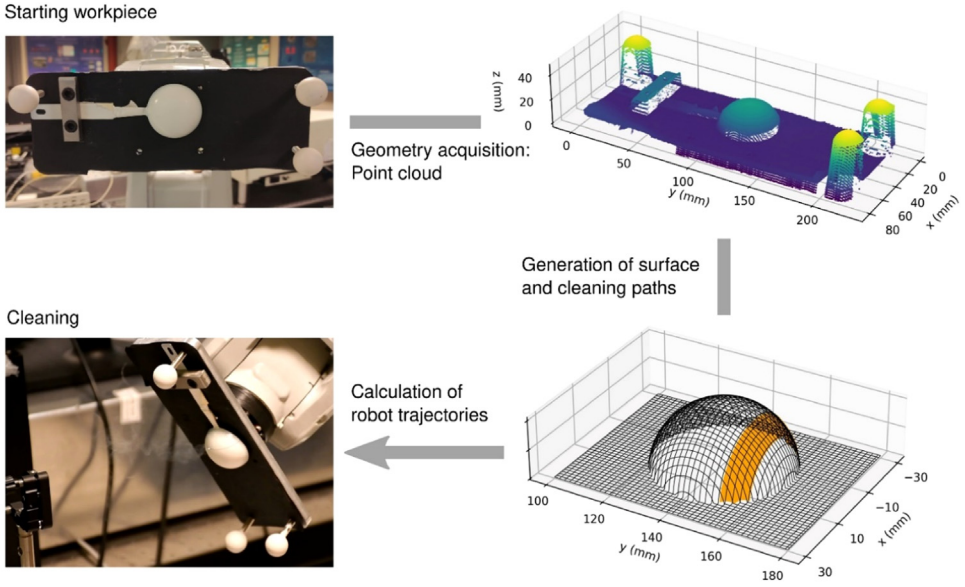


**Fig. 2.** Cleaning procedure. The geometry of the workpiece is scanned and a point cloud is obtained. A surface is generated from the point cloud and cleaning paths are calculated over it. The paths are transformed into robot trajectories and the workpiece is cleaned.

### 2.2. Experimental procedure

A digitizing procedure was developed and integrated with the laser cleaning system. Starting from an object with unknown geometry, the objective was to clean a specific region of its surface.

The procedure carried out to clean the surface of the object is divided into multiple stages. A simplified diagram of the procedure is shown in Fig. 2. First, the geometry of the object is acquired and digitized in the form of a point cloud. This is followed by a pre-processing step to filter the data and reduce noise. Next, the geometry of the workpiece is isolated in the point cloud and used to generate a smooth surface. Then, the curves corresponding to the laser cleaning paths are calculated over this surface. Finally, the robot tool trajectories corresponding to the laser paths are calculated and the cleaning is performed. Each of these steps will be explained in detail in the following sections.

#### 2.2.1. Obtaining the geometry of the workpiece

A laser scanner is used to obtain the geometry of the object. The scanner is placed in a fixed position and the object is held onto the end effector of the robot (Fig. 3). The laser profilometer works by projecting a laser line onto the surface to be measured and obtaining the coordinates of the points on the line by triangulation. Each measurement consists of a list of X-coordinates that correspond to the distance in the direction of the laser line and a list of Z-coordinates that correspond to the vertical distance between the scanner and the surface in the scanner coordinate system. According to the experimental setup used in this work, the robot is programmed to execute a horizontal rectilinear path on the XY plane of the world coordinate system, and following the Y direction of the scanner. While the robot moves the object through the laser beam, the scanner takes profile measurements at a constant acquisition frequency. The Y-coordinate of each profile is obtained by dividing the speed of the object by the acquisition frequency of the scanner. The origin of the Y-coordinate is arbitrary and depends on the instant in time when the acquisition of profiles begins.

The acquisition of the profiles is synchronized with the movement of the robot. The robot controller runs a TCP server that waits for movement orders from the control computer. The control computer sends the order to the robot to start the movement, and when it receives confirmation, it sends a command to the scanner to start taking profiles. When the movement is finished, the computer receives a signal from the robot and sends a stop command to the scanner. This procedure allows to easily perform scanning following custom trajectories. A simulation of the acquisition process is shown in VIDEO 1 https://doi.org/10.5281/zenodo.6628148.

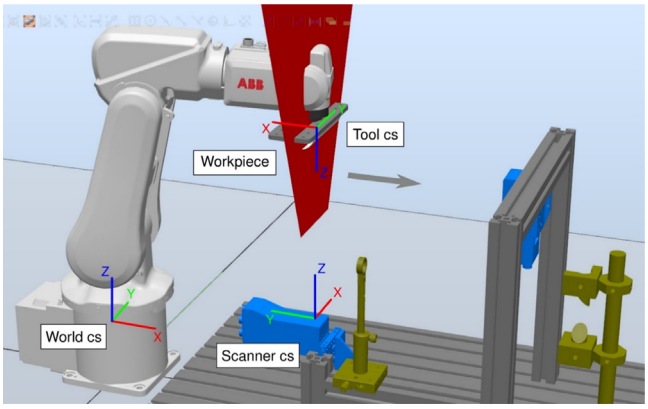


**Fig. 3.** Scanning setup. Coordinate systems involved are indicated (World cs, Scanner cs and Tool cs). The robot moves the workpiece following a horizontal rectilinear path at constant speed. The scanner is located below and projects a vertical beam on the workpiece, perpendicular to the movement direction. The coordinates of the surface are acquired line by line as the workpiece passes through the beam. A simulation of the acquisition process is shown in VIDEO 1 https://doi.org/10.5281/zenodo.6628148.

Once the measurement process is finished, the individual profiles, each one consisting of a set of X and Z coordinates and a single Y coordinate, are joined and a point cloud is obtained. If the point cloud can be considered as a range image, as is the case of a lot of common surfaces, the coordinates of the points are interpolated to a heightfield defined over a regular mesh in order to facilitate and accelerate the subsequent algorithms.

#### 2.2.2. Point cloud pre-processing and registration

The point cloud obtained in the previous step is referenced to the coordinate system of the scanner (Scanner cs in Fig. 3). Since the position and orientation of the scanner is known in the world coordinate system (World cs), the coordinates of the point cloud could be obtained in this last frame of reference simply by using the coordinate transformation between both coordinate frames. However, communication delays during the scanning procedure can cause errors on the assignment of the origin of Y-coordinates of the profiles, and, therefore, it is not practical

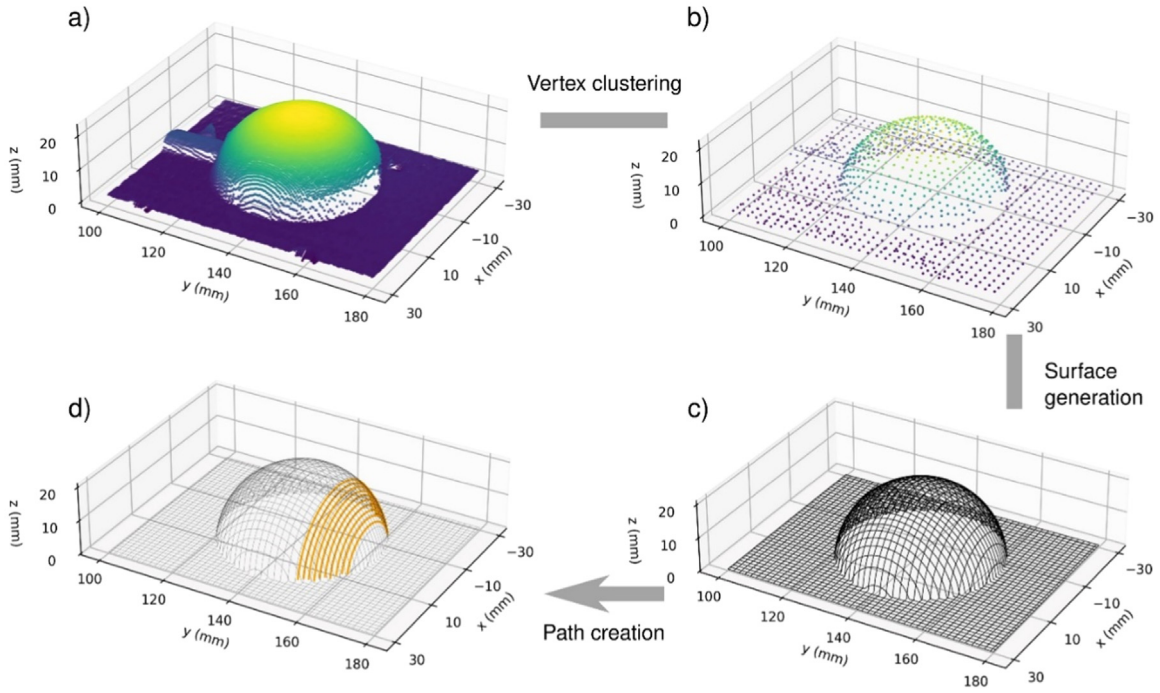


**Fig. 4.** Surface generation. a) The starting data is a point cloud; b) the raw point cloud is filtered using vertex clustering and the number of points is reduced; c). A surface is reconstructed from the points; d) cleaning paths are calculated on the surface.

to make the transformation directly. Since cleaning paths are defined in terms of tool coordinates relative to the world frame, to clean the object is enough to know its coordinates with respect to the robot end effector (Tool cs in Fig. 3).

To relate the coordinates of the point cloud to end effector of the robot, three spherical markers of known radius are placed on the plate that is attached to the end effector. The markers are arranged in a right triangle on the plane of the plate and the positions of their centers are known with respect to the tool frame. The advantage of using spherical markers over other types is that they can be detected and measured from different angles. When the surface is scanned and the point cloud is obtained, the coordinates of the centers of the spheres are found on the point cloud and their coordinates are related to their known coordinates in the tool frame. By knowing the coordinates of the three spheres in both reference frames, the transformation matrix between them can be calculated. To find the centers of the spheres in the point cloud, the following procedure is performed. First, a normal vector is estimated for every point of the cloud. In order to do this, a plane is fit to the neighborhood of each point using principal component analysis [38]. The normal of the point is approximated as the normal of this plane. Then, from each point of the point cloud, a vector is subtracted with the direction of the normal at each point and with length equal to the known radius of the spheres. The resultant point is the center of the hypothetical sphere of said radius that passes through each point. These points are aggregated in cells in a regular mesh. The cells with the highest density of points will correspond to the centers of the real spheres, since the points belonging to a valid sphere all generate the same center, while in an arbitrary region the resulting centers obtained are scattered. Therefore, the centers are located by looking for the local maxima in the grid. Once located, their positions are refined by means of a least-squares fit of the points in each region to a sphere.

### 2.2.3. Surface generation

The point cloud cannot be used directly as a basis for generating the cleaning paths due to the presence of noise. The noise present in the coordinates acquired by the scanner would be transformed into oscillations in the position and orientation of the robot tool. This would produce incorrect trajectories and in the case of large errors, trajectories that the robot could not execute. Therefore, it is necessary to transform the point cloud into a smooth surface from which curves can be drawn with continuity in both position and speed. The procedure for generating the surface from the point cloud is shown in Fig. 4. So that, before performing the surface reconstruction algorithm, vertex clustering (Fig. 4 b) is used on the point cloud to reduce the noise and thus improve the result of the reconstruction process to follow. At the same time, this step reduces the computational load during the reconstruction [39]. By this procedure, the points to be approximated are grouped into cells of a size determined by the user. The resulting points are the centroids of the points in each cell (for cells where there is any point). This method allows to mitigate noise at the expense of reducing spatial resolution. If the initial spatial resolution is greater than the resolution attainable by the robot and greater than the characteristic size of the details of interest on the surface, it is generally beneficial to perform this procedure. The resolution of the cells used in this step will be given by the desired minimum size of the details on the surface to be reconstructed.

Once the point cloud is pre-processed, the surface is reconstructed (Fig. 4c). In this work, two techniques are used to reconstruct surfaces from a point cloud. The method used depends on the characteristics of the surfaces of interest present in the point cloud. The techniques used were reconstruction with primitives using RANSAC and the APSS variant of moving least squares.

The RANSAC technique allows to extract simple primitive models present in the point cloud by means of a voting procedure [40]. The method starts from the hypothesis that a series of simple primitives exist inside the point set and it tries to find the best matches. In the case of this work, planes, spheres, cylinders, and cones were used. Through an iterative process, sets of random points are sampled from the point cloud and used to calculate the parameters of test models. These models are then tested against the entire dataset to know how many points are consistent with each model. The model with the highest number of points is accepted as valid. The points contained in the best model are extracted from the point cloud, and the search is repeated until the subset of points not explained by any model reaches a minimum. The main advantage of this reconstruction method is that the resulting surfaces do

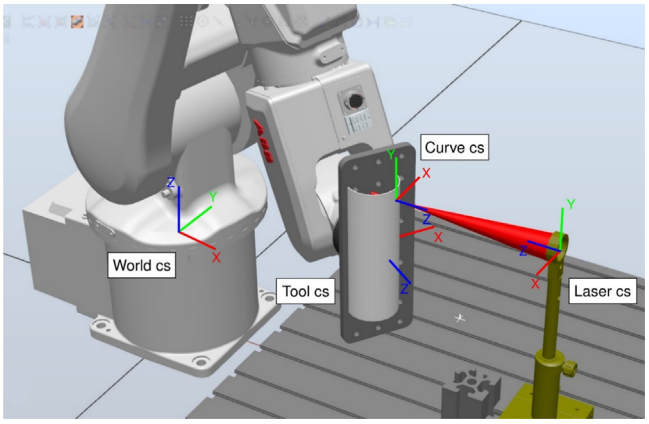


**Fig. 5.** Coordinate frames used in the cleaning system: World cs, Tool cs, Curve cs and Laser cs.

not contain any noise. This is very advantageous when generating robot paths on the surface. Therefore, this will be the preferred method if the workpiece, or at least the region subject to cleaning, is explained as the union of simple primitives.

If the surface to be reconstructed is complex and cannot be explained as a set of simple primitives, the method used is a variant of the moving least squares method, called Algebraic Point Set Surfaces (APSS) [41,42]. Moving least squares (MLS) is a family of methods in which the surface is reconstructed using local low-degree polynomials [43]. The neighborhood of each point of the point cloud is approximated by the best plane or polynomial in a weighted least-squares sense. These functions are weighted and therefore they are non-zero only in the vicinity of the point at which they are defined. The global surface is then recovered by evaluating the local functions in their influence domains. The local surfaces behave like a low pass filter, which makes them robust in the presence of noise. In the case of algebraic point surfaces, the approximation is carried out by algebraic spheres. The use of spheres improves the robustness of the method over planar approaches when dealing with areas of high curvature. For planar areas, the method simply degenerates to using planes as the approximating function.

It is important to note that both methods use least squares in one way or another to generate the resulting surfaces, either to approximate the primitives in the case of the RANSAC method or to approximate the local surfaces in the case of APSS. It is not feasible to apply methods that interpolate the points directly due to the experimental error present in the coordinates' values. The error also carries over to the calculation of normal, which will generally cause inadmissible errors in the position and orientation of the robotic tool.

### 2.2.4. Generation of robot trajectories

The area of the surface to be cleaned is filled with parallel curves that correspond to the paths that the laser follows on the surface (Fig. 4 d). To carry out the cleaning procedure, it is necessary to convert the laser paths on the surface to robot tool paths in the world frame. The tangent, normal, and binormal vectors of the surface curves define their characteristic frames. The frames of the curves can be related to the positions and orientations of the robot tool by solving the kinematic chain between their coordinate systems.

In Fig. 5, the world, tool, curve, and laser frames of references on the workspace are indicated. The world reference frame is located at the base of the robot. The object to be processed is anchored to a plate attached to the end effector of the robot. The tool of the robot is defined at the center of the plate and is referenced to the base of the robot. The curves defined on the surface of the object are referenced to the tool frame.

Let $T_{12}$ be the homogeneous transformation matrix that expresses the position and orientation of the frame 2 in the coordinates of frame 1. Then the pose of the robot tool in the world system are expressed as:

$$T_{wt} = T_{wl}\, T_{cl}^{-1}\, T_{tc}^{-1} \tag{1}$$

where $T_{wl}$ represents the transformation from the laser to the world frame and is defined by the position of the lens and the orientation of the beam, both known data. $T_{tc}$ are the surface curve frames expressed on the tool frame. The transformation matrix between the laser and the curve $T_{cl}$ is defined by the laser-surface incidence angle and the distance between the focus of the laser beam and the surface, both process parameters. Since the laser beam has radial symmetry, the rotation around the beam axis is used as an additional degree of freedom to increase the number of inverse kinematic solutions available for the robot motion.

The transformation (1) is applied to each of the $T_{cl}$ frames defined on the surface cleaning paths and the union of the resultant frames $T_{wt}$ defines the paths of the robot tool.

The robot used in this work, as well as most common manipulators, only executes moves along rectilinear and circular paths. Therefore, the tool paths are approximated using polylines, biarcs or a combination of both. Biarc interpolation is performed following the algorithms detailed in [44,45].

Finally, the joint angles of the robot for each of the poses $T_{wt}$ of the paths are obtained by solving the inverse kinematics of the manipulator. Since the robot is a six-axis serial manipulator with a spherical wrist, the resolution is carried out analytically [46,47]. For each pose, there exists multiple sets of solution angles that correspond to the different robot configurations. The only acceptable configurations are those that have a valid solution (angles within the mechanical limits of the robot) for all the poses of the path. In addition, it is necessary to check that, at no point, there are collisions between the object held in the end effector with the links of the robot.

In order to clean the curved surfaces used in this work, three different families of trajectories were used, from now on referred to as cases A, B, and C. Fig. 6 shows the diagram of the types of trajectories used for the case in which the object to be processed is a cylinder. In case A, the surface to be cleaned is considered to be flat. The robot moves the object following rectilinear paths with constant speed without change of orientation. Since the object is curved, neither the distance nor the angle of incidence laser-surface remains constant. This case represents the only methodology that would be possible if the object could only be moved in one plane. In case B, the distance between the laser focus and the surface is kept constant, but the angle of incidence is not. The piece describes curvilinear trajectories with constant orientation. This case would correspond to the positioner having three degrees of freedom of position, such as a coordinate table in XYZ or a three-axis Cartesian robot. In case C, both the distance and the angle of incidence laser-surface are kept constant. The piece describes curvilinear trajectories with variable orientation. This methodology can only be carried out with a positioner that has six degrees of freedom, such as the one used in this work. In cases B and C, the relative velocity between the laser beam and the surface must be kept constant to ensure that the energy deposited per unit area is uniform across the entire surface.

### 2.2.5. Laser cleaning

The process parameters for laser cleaning are laser power and frequency, scanning speed, hatching distance, diameter of the beam at the surface, and the angle of incidence between the laser beam and the surface. These parameters determine the density of energy that is deposited per unit area on the surface and the way in which the energy is distributed depending on whether the incidence is normal or oblique.

When the laser moves across the surface, the number of resulting spots per unit length is equal to the scanning speed multiplied by the frequency of the pulses. Although multiple combinations of speed and frequency result in the same number of pulses, the number of pulses per unit time will generally not be the same. This factor might be taken into account in long processes when using high fluence, since a heat affected zone may be developed on the surface of the material.

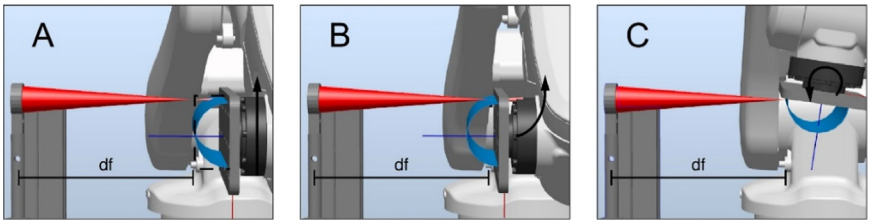


**Fig. 6.** Types of cleaning trajectories. A) 2D rectilinear path, neither distance to laser focus nor the angle of incidence with the beam are kept constant; B) 2.5D curvilinear path with constant orientation, distance to laser focus is maintained but not the angle of incidence; C) 3D curvilinear path with variable orientation, both the distance to the laser focus and the angle of incidence are kept constant.

**Table 1**
List of parameters used for the laser cleaning of the flat surface.

| | Number of repetitions $N_r$ | Frequency $f$ (kHz) | Distance focus-surface $dfs$ (mm) | Incidence angle $\theta$ (°) |
|---|---|---|---|---|
| | 1 | 20 | 0 | 0 |
| | 2 | 10 | 3 | 15 |
| | 3 | 5 | 4 | 30 |
| | 4 | 2.5 | 5 | 45 |
| | 5 | 1.25 | 6 | 50 |
| | 6 | 0.625 | - | 55 |
| | 7 | 0.3125 | - | - |
| **Constant values** | $f$=20 kHz $dfs$=3 mm $\theta$=0° | $N_r$=1 $dfs$=3 mm $\theta$=0° | $N_r$=1 $f$=20 kHz $\theta$=0° | $N_r$=1 $f$=20 kHz $dfs$=3 mm |

For practical purposes in the case of cleaning, scanning speed and laser frequency can be taken as independent parameters within reasonable windows. Thus, the frequency is fixed within the nominal limits of the laser system so that the scanning speed falls within the robot speed limits. It is convenient to adjust the frequency in such a way that the resultant scanning speed is not too high, since this could generate high accelerations that could produce vibrations in the system, thus potentially reducing the precision in the positioning of the laser on the surface. With the setup used in this work, using very high speeds produced vibrations in the table on which the lens is placed, which reduced the precision of the marking. Therefore, the scanning speeds used were selected within a range that avoided this problem.

### 2.3. Experimental case

#### 2.3.1. Characterization of cleaning of flat surfaces

A preliminary parametric study was carried out by cleaning flat pieces. The characterization of paint removal is easier in flat surfaces than in curved ones, so this experiment was used to find a set of suitable processing parameters for cleaning the material and paint under consideration. In addition, the effect of the laser-surface incidence angle and the focus-surface distance on the cleaning results were studied. The object to be cleaned was a 316L stainless steel plate of dimensions 100 mm × 50 mm × 5mm. The paint was removed on square areas of 5 mm × 5 mm, with the laser beam following parallel rectilinear trajectories at constant speed. Lines were overlapped in the direction perpendicular to the scanning direction until the area to be cleaned was completely covered. The distance between parallel lines was 30 μm. The parameters studied were: the number of irradiations over the area, the laser repetition rate or frequency, the laser-surface incidence angle, and the distance between the focus of the beam and the surface. The rest of the parameters were kept constant for all the areas: laser power 100% (4 W), scanning speed 20 mm·s$^{-1}$. The sets of parameters used are collected on Table 1. Once processed, the areas were visually inspected using a SMZ800 NIKON optical microscope and NIS-Elements software.

#### 2.3.2. Laser marking on curved surfaces

Laser marking tests were performed on a cylindrical surface ($r$=27 mm, $l$=150 mm) to analyze the dimensional accuracy of the system. The cylinder was covered with acetate paper and laser marking was conducted using the trajectories for cases A, B, and C indicated above. Characterization of curved surfaces in the microscope is not straightforward, but using the paper sheet that can be flattened, the position, size, and shape of the laser spots on the surface can be measured. The processing parameters used were 100% of nominal power, frequency $f$=200 Hz, scanning speed $v$=20 mm/s, and the laser focused at the surface. This results in a distance between consecutive spots of 100 μm in the scan direction. The lower laser frequency used with respect to the case of cleaning is intended to increase the distance between spots in order to facilitate their measurement. Since the speed of the robot is the same as in the case of cleaning, only the frequency is changed, the dimensional accuracy attained by the robot will be the same in both cases. For all cases, 10 parallel marking lines were made in a radial direction, with a separation between lines of 0.5 mm. The trajectories began at the top of the cylinder (0°) and ended at the base (90°).

#### 2.3.3. Cleaning of curved surfaces

Three types of metal objects were used to test the cleaning procedure: a cylinder, a sphere, and a tube clamp connector. They were painted with spray paint and left to dry for several days. The samples are shown in Fig. 7. The geometry of the samples was acquired following the procedure detailed in the previous sections. Then, regions were cleaned on each sample using the tool trajectory paths A, B, and C previously described.

The half-cylinder has a length of 150 mm and a diameter of 50 mm. The cleaning was performed on rectangular bands corresponding to radial sections of the cylinder. These areas were filled using parallel paths following the radial direction of the cylinder. The half-sphere has a diameter of 43 mm. For the cylinder, rectangular bands were processed. The tube clamp connector was selected to show the case of a more complex geometry. Rectangular bands were cleaned following two perpendicular directions, one along the long side of the object and another along the short side.

The process parameters used were the same for all the surfaces. The power was set to $P$=100% ($E_p$=49.7 μJ), the repetition rate to $f$=20 kHz, and the scanning speed to $v$=20 mm/s. The laser beam focus was set at a distance of 3 mm over the surface and the distance between cleaning paths was 30 μm. Videos of the cleaning processes (cases A, B, and C) of the cylindrical sample and of the tube clamp can be seen in VIDEO 2 https://doi.org/10.5281/zenodo.6628177 and VIDEO 3 https://doi.org/10.5281/zenodo.6628206, respectively.

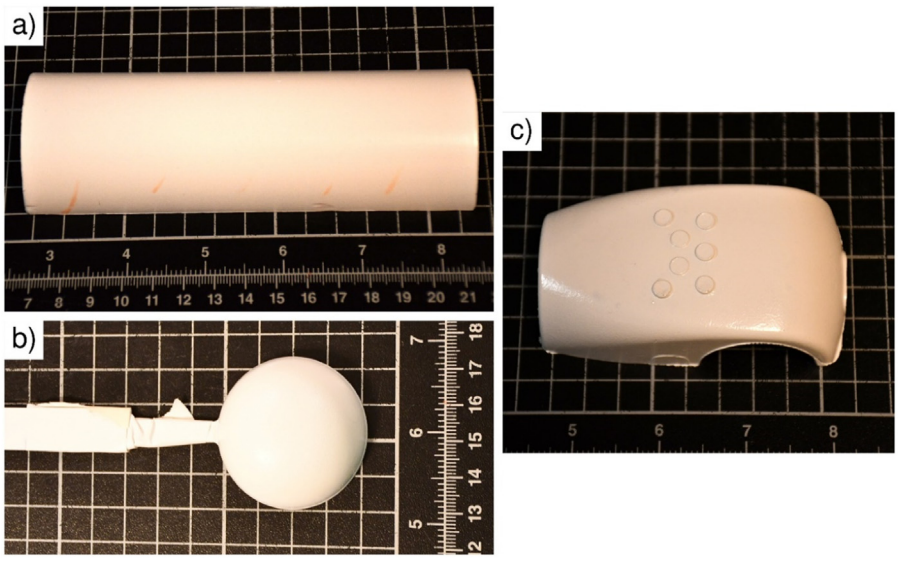


**Fig. 7.** Curved samples. a) Cylinder; b) sphere; c) tube clamp connector.

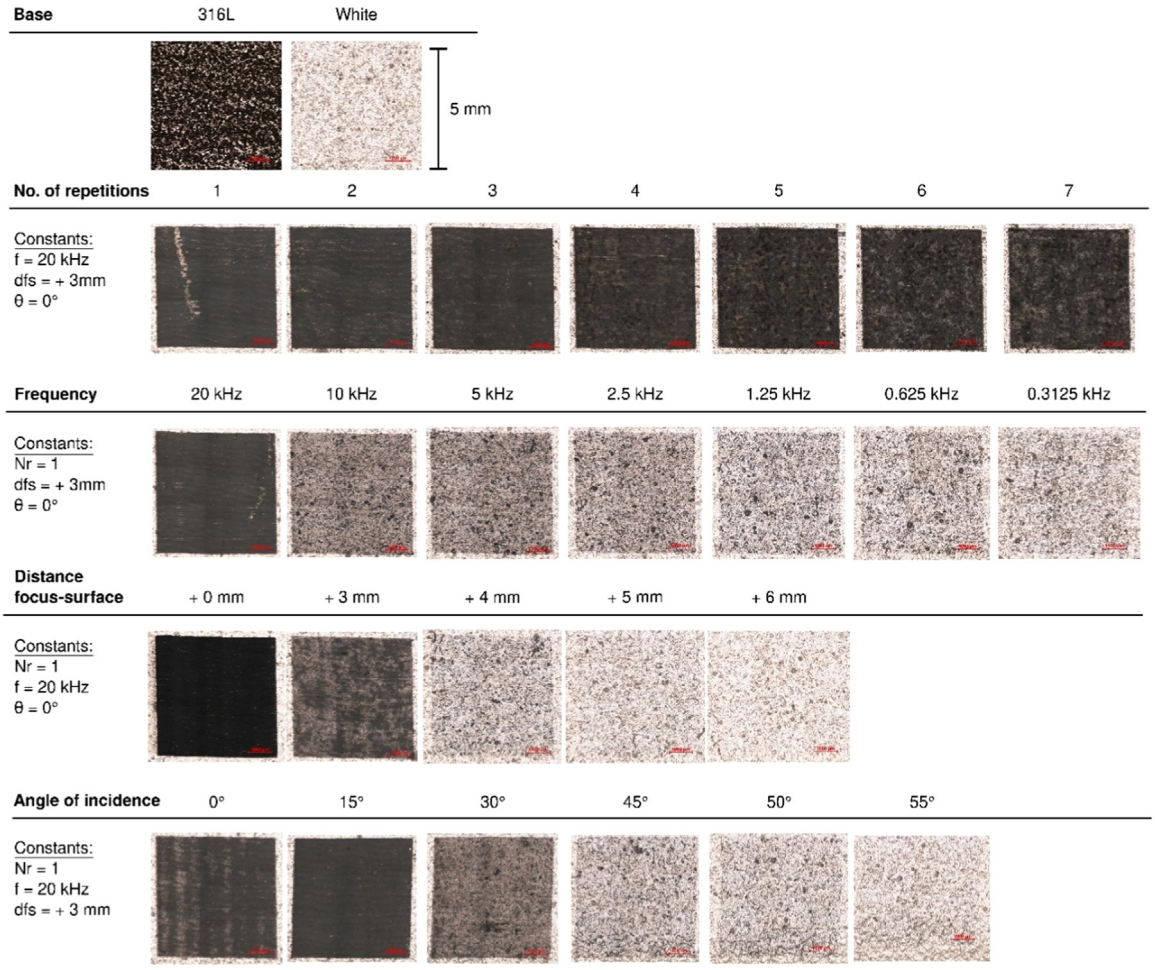


**Fig. 8.** Cleaned squares on the 316L flat plate. Each row shows the variation of a parameter.

## 3. Results and discussion

### 3.1. Characterization of paint removal on the flat surface

Images obtained by optical microscopy of the cleaned square areas on the flat plate are shown in Fig. 8. The upper object shows the appearance of the stainless-steel plate before and after painting. In the figure, each row represents the variation of one of the processing parameters, keeping the rest constant. The constant values used as the basis are $N_r$=1, $f$=20 kHz, $dfs$=+3 mm. The values chosen for the constant parameters represents a combination of parameters that result in adequate cleaning of the surface. The optimal value of repetitions seems to be 1 or

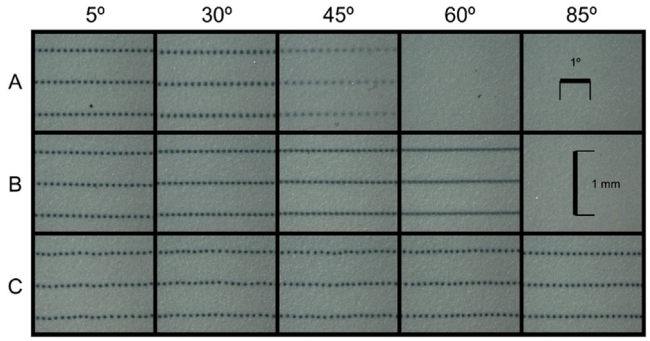


**Fig. 9.** Laser marking on the acetate paper placed on the cylinder for cases A, B, and C. From left to right, the images follow the trajectories from the top of the cylinder (0°) to the base (90°).

2. With 1 repetition, some small areas with white paint residues are noticed. As the number of repetitions increases, the surface is thermally affected and oxide begins to appear on multiple regions. Frequency has the effect of increasing (higher frequency) or decreasing (lower frequency) the number of spots per unit length in the scan direction. Therefore, the higher the frequency, the greater the energy deposited on the surface and, therefore, also the amount of material ablated. Of the values considered, the only frequency with satisfactory results is $f$=20 kHz. The areas for the remaining range of frequencies present a range of colors from greyish to whitish (from higher to lower frequency, respectively), which indicates that there is still a layer of paint on the surface. Regarding the distance from the focus of the beam to the surface, the cleaning is correct only for values of 0 mm and 3 mm above the surface. As the distance increases, the fluence decreases rapidly following the Gaussian divergence of the beam. This implies that with the optical system used, the cleaning of a curved surface will not be homogeneous when the distance between the lowest and the highest areas is greater than that range of distances. Regarding the angle of incidence, the cleaning is correct for angles of 0° and 15°. In the case of 30°, the cleaning is only objectual and for larger angles, most of the paint remains on the surface.

### 3.2. Evaluation and measurement of laser marking on the curved surfaces

Fig. 9 shows microscope images of the results of the laser marking on the cylinder covered by acetate paper for trajectories A, B, and C.

In case A, the marking was only carried out correctly in the range from 0° to 40°. In this case, the robot describes a rectilinear movement while the profile of the surface is an arc of circumference. Therefore, as the radial angle increases, the laser focus moves away from the surface, causing the absorbed energy to decrease and the spot marks to disappear quickly. Furthermore, since the scanning speed is constant, but the arc length of the path followed does not coincide with that of the surface profile, the distance between spots does not remain constant and increases as the radial angle increases. This phenomenon is not desirable in a cleaning process since the cleaning of paint or dirt would not be carried out homogeneously over the entire surface.

In case B, the trajectory of the robot followed an arc of circumference in order to maintain focus on the surface all the way. The result was a greater effective tagging region than in the previous case; however, as the radial angle increases, the incidence becomes more oblique, which causes a decrease in the energy absorbed at the surface and the disappearance of the spots. In this case, the distance between spots remained constant and equal to 100 μm. Towards the final range of angles (from 60°), the distance between spots seems to decrease. This is because, as the incidence of the laser becomes more oblique, the spots go from being perfect circles to ellipses, with their radius greater in the scanning direction. As the spots are more elongated in the direction of movement, the distance between the ends of the spots is smaller, but the distance between their centers remains the same.

In case C, the trajectory of the robot followed an arc such that the focus remained on the surface and the laser incidence was normal all the way. In this way, a correct marking was obtained for all angles.

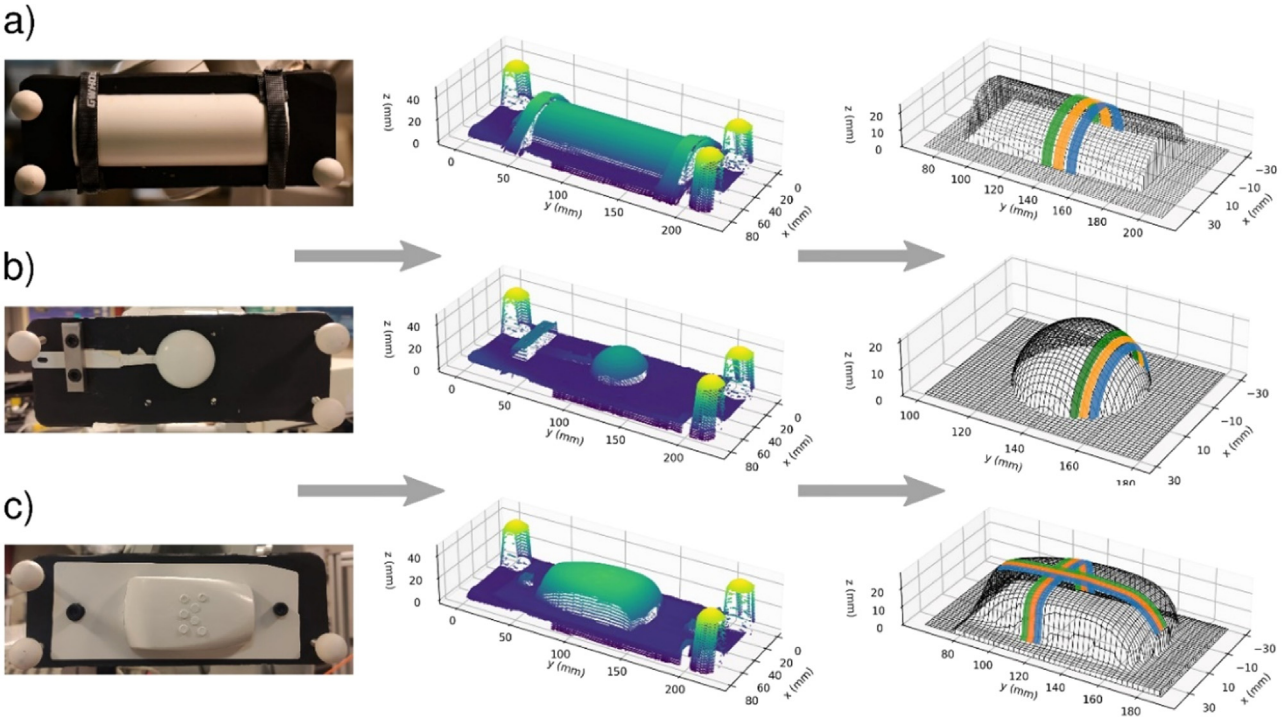


**Fig. 10.** Geometry reconstruction and calculation of cleaning paths for the 3D curved samples: a) cylinder, b) sphere and c) tube clamp connector.

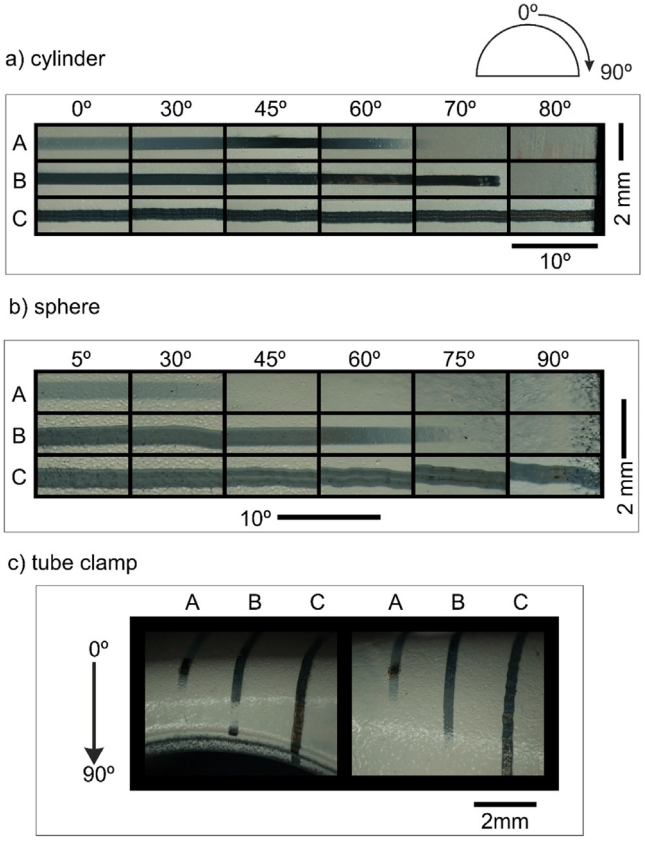


**Fig. 11.** Results of laser cleaning on the a) cylinder and b) sphere; c) tube clamp.

The distance was constant and equal to 100 μm as in the previous case. The spots maintained a circular shape with constant size throughout the entire route, which indicates that the distance and incidence remained constant as intended.

In all cases, the distances between the points obtained were kept according to the expected values for each trajectory, which indicates that the positioner speed behavior was correct. In the direction perpendicular to the movement, no large positional errors are observed and the spots appear to be correctly aligned. In case C, a small oscillation can be observed in the direction perpendicular to that of the movement. The fact that this is the only case in which the robot changes the orientation of the object seems to indicate that the precision of the robot in the position decreases slightly when it has to constantly change orientation and/or move more axes simultaneously.

### *3.3. Paint removal on curved surfaces*

In Fig. 10, the reconstructed surfaces of the pieces studied are shown. The point clouds obtained do not show appreciable errors and the noise level is low. The spherical markers were correctly detected in all cases. In the cases of the cylinder and the sphere, RANSAC was used to perform the reconstruction since these geometries can be approximated by simple primitives. The tube clamp presents more difficulties, as it contains almost vertical walls and unlike in the previous cases, its geometry cannot be treated as a simple primitive. Therefore, the surface was reconstructed using moving least squares. The algorithm smooths the sharp edges between the lateral walls and the top surface, which allowed transversal paths without discontinuities to be obtained. As an example, to give an idea of the duration of the process, in the case of the cylindrical piece (150 mm long and 50 mm in diameter), the time required to capture the surface was about 3 s (the profiles were taken at a scan speed of 30 mm/s and the acquisition length was about 90 mm, which corresponds to the width of the support and about 10 mm allowance). Regarding the processing time of the point cloud and generation of trajectories, it is about 10 s; that is, the duration of the processing prior to laser cleaning is less than 15 s.

The selected cleaning areas are shown over the surfaces. The areas were cleaned using the types of trajectories A, B, and C in blue, orange, and green respectively. The width of the grooves is magnified in the figures relative to the actual width so that they can be seen more clearly in the images. As it was intended to compare the cleaning result for the three cases, the cleaning bands were placed as close as possible to each other.

Fig. 11 shows the cleaning results for the different surfaces and types of trajectories. The discontinuities that can be observed within the cleaning grooves are the result of an imperfect alignment in the process of acquisition and assembly of the images and do not represent real discontinuities. For the sphere (Fig. 11b), in case A, a certain degree of cleaning is observed up to an angle of 20°. However, the paint layer was not completely removed since the surface has a whitish-gray tone. Between 20 and 30°, although the effect of the laser can still be appreciated, it worsens as the angle of incidence and the distance between the surface and the beam focus increase. For angles greater than 30°, there is no appreciable removal of paint. In case B, cleaning is satisfactory up to an angle of 50°. Unlike in case A, the paint is completely removed and the surface has a dark gray tone. From an angle of 50°, the effect of the laser began to attenuate and from 70° no change was seen in the paint layer. In case C, the paint layer was completely removed for the full range of angles. As the irradiation conditions are the same throughout the entire trajectory, the resultant paint removal was homogeneous throughout the entire range of angles. In case C, an oscillatory pattern was observed in the contour of the grooves. This phenomenon was already observed in the laser marking section, attributed to a decrease in the precision of the robot when it has to make changes in the orientation of the tool.

## 4. Conclusion

This research has developed a 6 DOF robot-assisted system for the automation of laser ablation processes in pieces with arbitrary geometry. The system incorporates an ultrashort pulse laser for processing, a robot that manipulates the piece, and a capturing system consisting of a laser profilometer that scans the object to generate a point cloud that determines the surface model. Laser paths are configured according to this model, and also include irradiation parameters for each point of the surface; scan speed, orientation, and focalization of the laser beam, in order to obtain a homogeneous processing throughout the entire surface. This is a full 3D solution that uses customized software which has been internally developed at our laboratory. The system has been applied for the elimination of painting coats on pieces with different geometry, whose results show that, for a working distance of 0 mm (that is, the laser focused at the object surface)) to 3 mm or for deviations of the normal incidence angle of the laser beam less than 15°, the effects in the paint removal cannot be appreciated; however, higher variations of both parameters have an outstanding effect, demonstrating the importance of a precise control over them.

It is important to point out that the results from this experiment can be extended to other processes, such as laser surface texturing, laser welding, or additive manufacturing, among others. Furthermore, the system configuration can be modified without changing this procedure so that the object stands in a static position while the robot manipulates the laser; in this sense, our group is working on the use of fiber lasers that can be easily guided by the robot, which improves the system's versatility and facilitates both the processing of big and fragile objects and the portability of the equipment

## Declaration of Competing Interest

The authors declare that they have no known competing financial interests or personal relationships that could have appeared to influence the work reported in this paper.

## CRediT authorship contribution statement

**Angel Rodríguez:** Methodology, Investigation, Formal analysis, Writing – original draft. **Ana J. López:** Conceptualization, Methodology, Investigation, Formal analysis, Resources, Writing – review & editing. **Javier Lamas:** Conceptualization, Methodology, Investigation, Formal analysis. **Alicia Moreno:** Investigation, Software. **Alberto Ramil:** Conceptualization, Methodology, Investigation, Software, Formal analysis, Resources, Data curation, Funding acquisition.

## Data availability

Data will be made available on request.

## Acknowledgments

Funding for the project was provided by the Ministry of Economy and Competitiveness- Spanish Government through project BIA2017-8589-R.

## References

[1] Luk'yanchuk B. Laser Cleaning. WORLD SCIENTIFIC; 2002. doi:101142/4952.
[2] Marimuthu S, Sezer HK, Kamara AM. Applications of Laser Cleaning Process in High Value Manufacturing Industries. Developments in Surface Contamination and Cleaning: Applications of Cleaning Techniques 2019:251–88. doi:10.1016/B978-0-12-815577-6.00007-4.
[3] Guan YC, Ng GKL, Zheng HY, Hong MH, Hong X, Zhang Z. Laser surface cleaning of carbonaceous deposits on diesel engine piston. Appl Surf Sci 2013;270:526–30. doi:10.1016/j.apsusc.2013.01.075.
[4] DiVito E, Peters OA, Olivi G. Effectiveness of the erbium:YAG laser and new design radial and stripped tips in removing the smear layer after root canal instrumentation. Lasers Med Sci 2012;27:273–80. doi:10.1007/s10103-010-0858-x.
[5] Al-Hashedi AA, Laurenti M, Benhamou V, Tamimi F. Decontamination of titanium implants using physical methods. Clin Oral Implants Res 2017;28:1013–21. doi:10.1111/CLR.12914.
[6] Delaporte P, Gastaud M, Marine W, Sentis M, Uteza O, Thouvenot P, et al. Radioactive oxide removal by XeCl laser. Appl Surf Sci 2002;197–198:826–30. doi:10.1016/S0169-4332(02)00456-7.
[7] Kumar A, Prasad M, Bhatt RB, Behere PG, Afzal M, Kumar A, et al. Laser shock cleaning of radioactive particulates from glass surface. Opt Lasers Eng 2014;57:114–20. doi:10.1016/j.optlaseng.2014.01.013.
[8] Siano S, Agresti J, Cacciari I, Ciofini D, Mascalchi M, Osticioli I, et al. Laser cleaning in conservation of stone, metal, and painted artifacts: state of the art and new insights on the use of the Nd:YAG lasers. Appl Phys A 2012;106:419–46. doi:10.1007/s00339-011-6690-8.
[9] Pouli P, Oujja M, Castillejo M. Practical issues in laser cleaning of stone and painted artefacts: optimisation procedures and side effects. Appl Phys A 2012;106:447–64. doi:10.1007/s00339-011-6696-2.
[10] López AJ, Rivas T, Lamas J, Ramil A, Yáñez A. Optimisation of laser removal of biological crusts in granites. Appl Phys A Mater Sci Process 2010;100:733–9. doi:10.1007/s00339-010-5652-x.
[11] Brand J, Rode AV, Madden S, Wain A, King PL, Rapp L. Ultrashort pulsed laser ablation of granite for stone conservation. Opt Laser Technol 2022;151:108057. doi:10.1016/J.OPTLASTEC.2022.108057.
[12] Oliveira V, Sharma SP, de Moura MFSF, Moreira RDF, Vilar R. Surface treatment of CFRP composites using femtosecond laser radiation. Opt Lasers Eng 2017;94:37–43. doi:10.1016/J.OPTLASENG.2017.02.011.
[13] Rivas T, Lopez AJ, Ramil A, Pozo S, Fiorucci MP, Silanes MEL de, et al. Comparative study of ornamental granite cleaning using femtosecond and nanosecond pulsed lasers. Appl Surf Sci 2013;278:226–33. doi:10.1016/j.apsusc.2012.12.038.
[14] Fiorucci MP, López AJ, Ramil A, Pozo S, Rivas T. Optimization of graffiti removal on natural stone by means of high repetition rate UV laser. Appl Surf Sci 2013;278:268–72. doi:10.1016/j.apsusc.2012.10.092.
[15] Overmeyer L, Duesing JF, Suttmann O, Stute U. Laser patterning of thin film sensors on 3-D surfaces. CIRP Ann 2012;61:215–18. doi:10.1016/j.cirp.2012.03.087.
[16] Ostholt R, Willenborg E, Wissenbach K. Laser polishing of metallic freeform surfaces. In: International Congress on Applications of Lasers & Electro-Optics. Laser Institute of America; 2010. p. 597–603. doi:10.2351/1.5062086.
[17] Ramil A, Pozo-Antonio JS, Fiorucci MP, López AJ, Rivas T. Detection of the optimal laser fluence ranges to clean graffiti on silicates. Constr Build Mater 2017;148. doi:10.1016/j.conbuildmat.2017.05.035.
[18] López AJ, Ramil A, Pozo-Antonio JS, Rivas T, Pereira D. Ultrafast Laser Surface Texturing: A Sustainable Tool to Modify Wettability Properties of Marble. Sustainability 2019;11:4079. doi:10.3390/su11154079.
[19] Fiorucci MP, López AJ, Ramil A. Comparative study of surface structuring of biometals by UV nanosecond Nd:YVO4 laser. Int J Adv Manuf Tech 2014;75:515–21. doi:10.1007/s00170-014-6164-1.
[20] Moreno A, López AJ, Lamas J, Ramil A. Femtosecond pulsed laser ablation for paint removal at oblique illumination: effect of the incidence angle. Optik 2022:169428. doi:10.1016/J.IJLEO.2022.169428.
[21] Jiang M, Wang X, Ke S, Zhang F, Zeng X. Large scale layering laser surface texturing system based on high speed optical scanners and gantry machine tool. Rob Comput Integr Manuf 2017;48:113–20. doi:10.1016/j.rcim.2017.03.005.
[22] Batal A, Michalek A, Penchev P, Kupisiewicz A, Dimov S. Laser processing of freeform surfaces: A new approach based on an efficient workpiece partitioning strategy. Int J Mach Tools Manuf 2020;156:103593. doi:10.1016/j.ijmachtools.2020.103593.
[23] Cuccolini G, Orazi L, Fortunato A. 5 Axes computer aided laser milling. Opt Lasers Eng 2013;51:749–60. doi:10.1016/j.optlaseng.2013.01.015.
[24] Wang X, Duan J, Jiang M, Ke S, Wu B, Zeng X. Study of laser precision ablating texture patterns on large-scale freeform surface. Int J Adv Manuf Tech 2017;92:4571–81. doi:10.1007/s00170-017-0413-z.
[25] Geng Z, Bidanda B. Review of reverse engineering systems – current state of the art. In: Virtual and Physical Prototyping, 12; 2017. p. 161–72. doi:10.1080/17452759.2017.1302787.
[26] Ribo M, Brandner M. State of the art on vision-based structured light systems for 3D measurements. In: International Workshop on Robotic Sensors: Robotic and Sensor Environments, 2005. IEEE; 2005. p. 2–6. doi:10.1109/ROSE.2005.1588327.
[27] Weyrich T, Pauly M, Keiser R, Heinzle S, Scandella S, Gross M. Post-processing of Scanned 3D Surface Data. In: Alexa M, Gross M, Pfister H, Rusinkiewicz S, editors. SPBG'04 Symposium on Point - Based Graphics 2004. The Eurographics Association; 2004. p. 85–94. doi:10.2312/SPBG/SPBG04/085-094.
[28] Berger M, Tagliasacchi A, Seversky LM, Alliez P, Guennebaud G, Levine JA, et al. A Survey of Surface Reconstruction from Point Clouds. Comput Graphics Forum 2017;36:301–29. doi:10.1111/cgf.12802.
[29] López AJ, Lamas J, Pozo-Antonio JS, Rivas T, Ramil A. Development of processing strategies for 3D controlled laser ablation: Application to the cleaning of stonework surfaces. Opt Lasers Eng 2020;126:105897. doi:10.1016/J.OPTLASENG.2019.105897.
[30] Zhang X, Li W, Liou F. Damage detection and reconstruction algorithm in repairing compressor blade by direct metal deposition. Int J Adv Manuf Tech 2018;95:2393–404. doi:10.1007/s00170-017-1413-8.
[31] Wilson JM, Piya C, Shin YC, Zhao F, Ramani K. Remanufacturing of turbine blades by laser direct deposition with its energy and environmental impact analysis. J Cleaner Prod 2014;80:170–8. doi:10.1016/j.jclepro.2014.05.084.
[32] Garmendia I, Leunda J, Pujana J, Lamikiz A. In-process height control during laser metal deposition based on structured light 3D scanning. Procedia CIRP 2018;68:375–80. doi:10.1016/J.PROCIR.2017.12.098.
[33] Heralić A, Christiansson A-K, Lennartson B. Height control of laser metal-wire deposition based on iterative learning control and 3D scanning. Opt Lasers Eng 2012;50:1230–41. doi:10.1016/j.optlaseng.2012.03.016.
[34] Nguyen HC, Lee BR. Laser-vision-based quality inspection system for small-bead laser welding. Int J Precis Eng Manuf 2014 2014;15:415–23 15:3. doi:10.1007/S12541-014-0352-7.
[35] Li X, Ren X, Mei X, Liu B, Wang W, Wang X. In situ three-dimensional laser machining system integrating in situ measurement, reconstruction, parameterization, and texture mapping. Int J Adv Manuf Tech 2020;111:673–84. doi:10.1007/s00170-020-06016-z.
[36] Diaci J, Bračun D, Gorkič A, Možina J. Rapid and flexible laser marking and engraving of tilted and curved surfaces. Opt Lasers Eng 2011;49:195–9. doi:10.1016/j.optlaseng.2010.09.003.
[37] Qi L, Zhang Y, Wang S, Tang Z, Yang H, Zhang X. Laser cutting of irregular shape object based on stereo vision laser galvanometric scanning system. Opt Lasers Eng 2015;68:180–7. doi:10.1016/j.optlaseng.2014.12.007.
[38] Klasing K, Althoff D, Wollherr D, Buss M. Comparison of surface normal estimation methods for range sensing applications. In: 2009 IEEE International Conference on Robotics and Automation. IEEE; 2009. p. 3206–11. doi:10.1109/ROBOT.2009.5152493.
[39] Martin R, Stroud I, Marshall A. Data reduction for reverse engineering. The mathematics of surfaces. In: Proceedings of the 7th IMA conference; 1996. p. 1996.
[40] Schnabel R, Wahl R, Klein R. Efficient RANSAC for Point-Cloud Shape Detection. Comput Graphics Forum 2007;26:214–26. doi:10.1111/j.1467-8659.2007.01016.x.
[41] Guennebaud G, Gross M. Algebraic point set surfaces. In: Proceedings of the ACM SIGGRAPH Conference on Computer Graphics; 2007.
[42] Guennebaud G, Germann M, Gross M. Dynamic Sampling and Rendering of Algebraic Point Set Surfaces. Comput Graphics Forum 2008;27:653–62. doi:10.1111/j.1467-8659.2008.01163.x.
[43] Cheng Z-Q, Wang YZ, Li B, Kai X, Dang G. Survey of Methods for Moving Least Squares Surfaces; 2008. VG/PBG@SIGGRAPH.
[44] Sabin M. The use of piecewise forms for the numerical representation of shape. Budapest, 1976.
[45] Deng C, Ma W. A biarc based subdivision scheme for space curve interpolation. Comp Aid Geomet Des 2014;31:656–73. doi:10.1016/j.cagd.2014.07.003.
[46] Craig JJ. Introduction to robotics: mechanics and control 3/E. 3rd ed. India: Pearson Education; 2009.
[47] Corke P. Robotics, Vision and Control, 73. Berlin, Heidelberg: Springer Berlin Heidelberg; 2011. doi:10.1007/978-3-642-20144-8.